Desalination and Water Treatment
www.deswater.com

doi: 10.5004/dwt.2021.27651

240 (2021) 14–23
November

Comparison of the performance of three nanofiltration membranes for the reduction of fluoride ions: application of the Spiegler–Kedem and Steric Hindrance Pore Models

Mustapha Tahaikt[a], Fatima Elazhar[a], Idrisse Mohamed[a], Hajar Zeggar[a], Mohamed Taky[a,b,*], Azzeddine Elmidaoui[a]

[a]*Laboratory of Advanced Materials and Process Engineering, Faculty of Sciences, Ibn Tofail University, P.O. Box: 1246, Kenitra, Morocco, emails: mohamed.taky@uit.ac.ma (M. Taky), mustapha.tahaikt@uit.ac.ma (M. Tahaikt), fatima.elazhar@uit.ac.ma (F. Elazhar), mohamed.idrisse@uit.ac.ma (I. Mohamed), zeggar.hajar@uit.ac.ma (H. Zeggar), elmidaoui@uit.ac.ma (A. Elmidaoui)*
[b]*International Water Research Institute, Mohammed VI Polytechnic University, Benguerir, Lot 660, Hay Moulay Rachid Ben Guerir, 43150 – Morocco*

Received 11 May 2021; Accepted 23 July 2021

ABSTRACT

High levels of fluoride in the aquatic environment are often detected in several countries, in particular Morocco. Due to the adverse health effects of these ions (dental and bone fluorosis), the World Health Organization (WHO) has set the maximum permissible concentration in drinking water at 1.5 mg/L. The objective of this work is to study the influence of initial concentration and pressure on the removal of fluoride (F^-) ions by nanofiltration (NF) from groundwater doped with NaF. Three membranes are tested namely NF90, NF270 and TR60. To understand the transfer mechanisms in these three NF membranes and for different initial concentrations, the solute flow by convection and the flow by diffusion are calculated. In addition, two mathematical models are used. The Spiegler–Kedem model is applied to determine the reflection coefficient σ and the solute permeability coefficient P_s at different initial concentrations. The Steric Hindrance Pore (SHP) model is applied to determine the mean pore radius for the membranes studied. The results show that there is no significant effect of the initial concentration and the applied pressure on the concentration of fluoride ions in the permeate for the NF90 membrane. On the other hand, the other two membranes NF270 and TR60, exhibit similar behaviors with respect to fluoride ions. A value exceeding the allowed limit of F^- is observed from 6 ppm for NF270 and from 5 ppm for TR60. The C_{conv} and J_{diff} increase with the increase in the initial concentration of fluoride ions. NF270 and TR60 membrane involve diffusion and convection mechanisms. For NF90 the diffusion mechanism is predominant. The reflection coefficient σ obtained for NF90 is close to unity; the TR60 and NF90 behave a little differently, with an increase in the fluoride content. The pore size (r_p) determined by the SHP model, follows the following order:

$$r_p(\text{TR60}) > r_p(\text{NF270}) > r_p(\text{NF90})$$

Keywords: Fluoride removal; Nanofiltration; Mass transport mechanisms; Spiegler–Kedem model; Steric Hindrance Pore Model

* Corresponding author.

Presented at the Second International Symposium on Nanomaterials and Membrane Science for Water, Energy and Environment (SNMS-2021), June 1–2, 2022, Tangier, Morocco

1. Introduction

Water is an essential natural resource to support life and the environment which we have always believed to be abundantly available and free from nature. However, the chemical composition of the surface or subsoil is one of the main factors on which the suitability of water for domestic, industrial or agricultural purposes depends [1]. Recent UNICEF and World Health Organization (WHO) reports have confirmed that 748 million people have no access to safe water of proper quality, while more than 1.8 billion people use water contaminated with feces for potable purposes [2].

The presence of several natural and anthropogenic elements and compounds, such as fluorides, arsenic, nitrates, sulfates, iron, manganese, chlorides, selenium, heavy metals and radioactive substances may significantly affect water quality and cause harmful health effects [2–4].

Fluoride is one of the trace elements essential for normal human growth [5]. However, the excessive ingestion of fluoride through drinking water causes dental, skeletal, and non-skeletal forms of fluorosis [6,7]. Fluoride in drinking water can be either beneficial or detrimental to health depending on points concentration. The WHO accepted the maximum fluoride concentration in drinking water as 1.5 mg/L [1]. On the contrary, excess concentration (3–6 mg/L) of fluoride can have an adverse effect on bones and dental (dental and skeletal fluorosis [8]. Besides, fluoride anions also exert adverse influences on the nervous system, digestive system and urinary system [9]. In many regions of Morocco, the fluoride content exceeds acceptable standards. In the plateau of Ben Guerir (Centre of Morocco), the harmful effect of dental fluorosis is widespread among the population supplied directly from wells [10].

Hence, in this direction, over the years, a plethora of conventional methods have been implemented for defluoridation of water namely as adsorption [3,9,11], ion-exchange [12], electrodialysis [9], precipitation/coagulation [13] and driven pressure membrane technologies [10] have been implemented.

Among these membrane-based technologies, nanofiltration (NF) stands to be one the most effective to remove a number of other contaminants also from groundwater at a relatively low transmembrane pressure (TMP) [14]. Many researchers have studied the rejection of different salts using different types of NF membrane and showed that the rejection values depend on the type of NF membranes used [15]. In a previous study, Tahaikt et al. [16] reported the usage of "dense" NF membrane such as NF70 and NF90 and "loose" NF membrane including NF270, NF400, and TR60 for fluoride rejection from model solutions.

Tahaikt et al. [10] compared the effectiveness of removing fluoride from water using three commercial polyamide NF membranes: NF90 (FilmTec, USA), NF270 (FilmTec, USA) and TR60 (Toray, Japan). They showed that fluoride rejection depends on the initial fluoride content in the feed. This rejection exceeds 74% for NF270 and TR60, and for NF90, the rejection exceeds 98% with less dependence on the initial fluoride concentration in the feed. Shen and Schäfer [17] studied fluoride and natural organic matter removal in a small stirred laboratory cell. They conducted experiments with 22 samples of natural waters from Tanzania and 6 NF/reverse osmosis (RO) membranes. The fluoride concentration in the studied samples was ranged between 2.6 and 239.9 mg/L. The Dow FilmTec (USA) NF90, BW30 and BW30-LE membranes showed the highest fluoride rejection (>95% and up to 50% recovery). This result was attributed to size exclusion due to fluoride ion hydration. Ben Nasr et al. [18] compared fluoride rejection performances of two commercial NF membranes (NF5 and NF9) from groundwater. The authors showed that NF5 and NF9 membrane exhibit widely different fluoride rejection, 57% and 88% respectively. The fluoride ion concentration in permeate was observed to be 1.45 mg/L (F^- rejection: 57%) and 0.38 mg/L (F^- rejection: 88%), respectively. According to a previous study [19,20], the "dense" NF membranes are recommended for surface and groundwater treatment because they remove a high percentage of salts and organics whereas the "loose" NF membranes are appropriate in water treatment where only good organic matter rejection is expected with partial softening.

Shen et al. [21] carried out field trials with brackish water (BW) from a borehole located at a rural school in northern Tanzania, characterized by high salinity levels (TDS = 3,632 mg/L) and very high fluoride concentrations ($[F^-]$ = 47.6 mg/L). Experiments were conducted with a solar-powered pilot-scale unit. Both RO membranes and NF90 membranes were able to remove the fluoride to comply with the WHO limit of 1.5 mg/L, whereas NF270 could not comply with this limit (fluoride in permeate: 14.2 mg/L) due to the fact that it is a "looser" NF-membrane in comparison to NF90. Tahaikt et al. [10] studied the performance of three different membranes, NF90 and two RO membranes (BW30 and TM710) with an industrial pilot. For an initial feed concentration of 2.32 ppm and for conversion rates of 84% for NF90, 80% for TM710 and BW30LE, the content of F^- in the obtained permeate did not exceed 0.5 ppm (0.5 ppm for NF90, 0.3 for TM710 and BW30LE).

Presently, the retention mechanism of the NF membrane process is complicated and not yet fully known. Extensive work has been done and is still being conducted to investigate transfer and retention mechanisms including NF processes modeling. Many models were constructed to describe and predict the flux and retention of various charged and uncharged species by NF membrane and can be used for the determination of membrane characteristics including effective thickness, porosity ratio, pore size, membrane charge density, and prediction of the NF processes performance [8].

The objective of this work is based on the performance of three NF membranes, namely TR60, NF270 and NF90 in the reduction of fluoride ions, for different initial concentrations. The Kedem–Katchalsky and Spiegler–Kedem models are applied to determine the solute flow by convection and the flow by diffusion and the model constants, namely the reflection coefficient σ and the permeability coefficient P_s [22,23], in order to determine the influence of the initial fluoride ion content on these constants; for the three membranes used. In addition, the Steric Hindrance Pore (SHP) model is applied to determine the radius of the pore.

2. Method and analysis

The experiments are carried out on an nanofiltration/reverse osmosis (NF/RO) pilot installation (E 3039) supplied by TIA Company (Technologies Industrielles Appliquées, France). Fig. 1 gives the diagram of the pilot installation used. The TMP is varied from 5 to 40 bar with manual valves. The pilot plant is equipped with two spiral wound modules operating in series.

The module contains one element. The pressure drop is approximately 2 bars corresponding to 1 bar of each module. The configurations tested are: single pass, double pass and batch configuration provided. Table 1 gives the characteristics of the commercial membranes used.

The experiments are performed at 30°C. After analysis, the membranes are cleaned with alkaline and acidic cleaning solutions according to the manufacturer's recommendations. Studying the performance of membranes tested in a wide range of concentrations, experiments are conducted on groundwater doped with NaF to reach 1, 5, 10, 15 and 20 ppm fluoride. The characteristics of untreated water are shown in Table 2.

Samples of permeate are collected and fluoride ion concentrations are determined potentiometrically using a selective electrode and using an ionometer type HANNA Instruments, GLP Microprocessor pH/Ion Meter, Model pH-301. Other water parameters are determined analytically following standard methods previously described [10,16].

Parameters are tracked such as ion rejection (R) and permeate flux (J_v) are defined by the following analytical expressions:

$$R = 1 - \frac{C_p}{C_o} \cdot 100 \tag{1}$$

$$J_v\left(\mathrm{m}^3 \cdot \mathrm{m}^{-2} \cdot \mathrm{s}^{-1}\right) = \frac{Q_p\left(\mathrm{m}^3 \cdot \mathrm{s}^{-1}\right)}{S\left(\mathrm{m}^2\right)} \tag{2}$$

where C_o, C_p, S and Q are the feed concentration, the permeate concentration, the area and the volume flow, respectively.

3. Mathematical models

3.1. Kedem–Katchalsky and Spiegler–Kedem models

To determine the diffusive and convective transfer mechanism terms, Kedem–Katchalsky and Spiegler–Kedem models have been proposed.

3.2. Mass transfer mechanism

The NF membrane is the seat of two transfer mechanisms: diffusion and convection. Therefore, the balance tells us that the flow of solute J_s is given by the following relations:

$$J_s = J_{\text{diff}} + J_p \cdot C_{\text{conv}} \tag{3}$$

$$J_s = C_P \cdot J_p \tag{4}$$

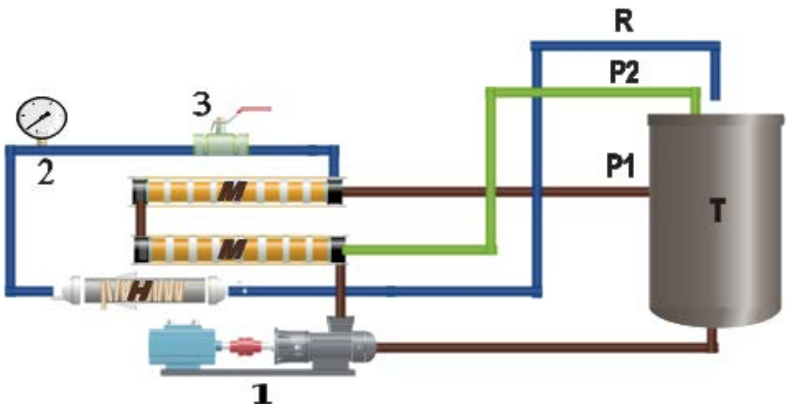

Fig. 1. Schematic diagram of the nanofiltration/reverse osmosis pilot plant. T: tank; M: nanofiltration module; P: permeate recirculation; R: retentate recirculation; H: heat exchanger; 1: high-pressure pump; 2: pressure sensor; 3: pressure regulation valves.

Table 1
Characteristics of the membranes used

Membrane	Area (m^2)	Salt rejection (%)	P_{max} (bar)	pH	Material
NF90*4040	7.6	97%	41	3–10	Polyamide
NF270*4040	7.6	>97.0%	41	3–10	Polyamide
TR60*4040	6.8	–	10	3–10	Polyamide

Salt rejection based on the following test conditions 2,000 ppm $MgSO_4$, 77°F (25°C), and 15% recovery rate at the pressure 4.8 bar.
Salt rejection based on the following test conditions 2,000 ppm NaCl, 77°F (25°C), and 15% recovery rate at the pressure 10 bar.
Salt rejection based on the following test conditions 2,000 ppm NaCl, 77°F (25°C), and 15% recovery rate at the pressure 15.5 bar.

Table 2
Characteristic of the feed water

Parameter	Feed water	Moroccan Guidelines	WHO Guidelines
Temperature, °C	29	–	25
Turbidity, NTU	<2	<5	–
pH	7.41	6–9.2	6.5–8.5
pHs	7.80	–	–
Electric conductivity, μS/cm	1,492	2,700	–
Hardness, mg/L $CaCO_3$	440	500	500
Alkalinity, mg/L $CaCO_3$	320	200	–
Fluoride, mg/L	1, 5, 10, 15, 20	1.5	1.5
Sulfate, mg/L	116	200	200
Chloride, mg/L	560	350	250

By dividing each member by J_p we obtain an affine map [Eq. (5)] with C_p the y-intercept and J_{diff} the slope of the line, given by the following relation:

$$J_{\text{diff}} \cdot \left(\frac{1}{J_p}\right) + C_{\text{conv}} = C_P \tag{5}$$

To better understand the phenomena of material transfer through NF membranes, other parameters were determined from the model proposed by Spiegler–Kedem (SK).

The SK model which is based on irreversible thermodynamics considers the membrane as a "black box". By introducing the local transport coefficients, SK obtained the following equations:

$$J_v = -L_p\left(\frac{dp}{dx} - \sigma\frac{d\pi}{dx}\right) \tag{6}$$

$$J_s = -\overline{P}\frac{dC_s}{dx} + (1-\sigma)C_s J_v \tag{7}$$

where L_p, p, x, π, $\overline{P}$, C_s and σ represent respectively the hydraulic permeability, the pressure, the distance, the osmotic pressure, the local permeability of the solute, the solute concentration in the membrane and the reflection coefficient. According to Eq. (7), the solute flux is the sum of diffusive and convective terms. Transport of the solute by convection is due to an applied pressure gradient across the membrane. The concentration difference on the membrane side and the permeate result in transport by diffusion.

The integration of these equations combined with the relation of the rejection and by considering the limiting conditions of the problem (for $x = 0$, $C_m = C_f$ and for $x = \Delta x$, $C_m = C_p$) lead to the following relations:

$$J_v = L_p(\Delta P - \sigma\Delta\pi) \tag{8}$$

$$R = 1 - \frac{C_p}{C_f} = \frac{\sigma(1-F)}{1-\sigma F} \tag{9}$$

where $F = \exp\left(\frac{(1-\sigma)J_v}{P_s}\right)$.

where ΔP: TMP, $\Delta\pi$: difference in osmotic pressure on either side of the membrane (bar), C_o, C_p, C_m: concentrations in feed, permeate and in the membrane respectively, L_p: hydraulic permeability of the membrane, σ: reflection coefficient, P_s: solute permeability and Δx is the membrane thickness [14].

The following assumptions were made while using the SK model in this research:

- The driving forces are pressure and concentration gradients.
- The model predicts the transport of the solute and solvent through the membrane irrespective of the type of solute, charge, solvent, and membrane [24].

3.3. Steric Hindrance Pore model

The SHP is a model correlating structure to transport. The parameters which were described by the preceding analytical equations are not the only ones to give relevant information on the behavior of membranes of NF. The SHP model has been proposed to determine the pore size r_p and the ratio of porosity and membrane thickness $A_K/\Delta X$. NF membrane characteristics such as pore size, effective thickness/porosity ratio, and membrane charge density are evaluated by a solute (uncharged) and salt rejection experiments using pore models such as the SHP model [25].

The structural parameters of the membranes were estimated using the SHP model developed by Nakao and Kimura for the separation of aqueous solutions from a single organic solute by ultrafiltration membranes and have subsequently been used successfully for NF membranes [8]. Depending on the model, transport of spherical ions through cylindrical pores by frictional forces and steric effect are taken into account. According to this model, the membrane parameters σ and P_s are given in the following equations:

$$\sigma = 1 - S_F\left(1 + \left(\frac{16}{9}\right)q^2\right. \tag{10}$$

$$P_S = D_{\text{diff}} \times S_D\left(\frac{A_K}{\Delta X}\right) \tag{11}$$

$$S_D = (1-q)^2 \text{ and } S_F = 2(1-q)^2 - (1-q)^4 \quad (12)$$

$$q = \frac{r_s}{r_p} \quad (13)$$

where S_D and S_F are the steric hindrance factors for diffusion and convection respectively. D_{diff} is diffusion constant, $A_K/\Delta X$ is the ratio of membrane porosity to membrane thickness, r_s is the Stokes radius of the solute, and r_p is the pore radius.

4. Results and discussion

4.1. Influence of the initial concentration and the applied pressure

Fig. 2 gives, for the membranes tested and for different initial feed concentrations, the variation of the permeate concentration of fluoride as a function of TMP, and gives the variations of the average flux, conductivity and pH of the permeate, in all the defluoridation operations.

Analysis of these results shows that: the permeate flux increases almost linearly with TMP according to Darcy's law.

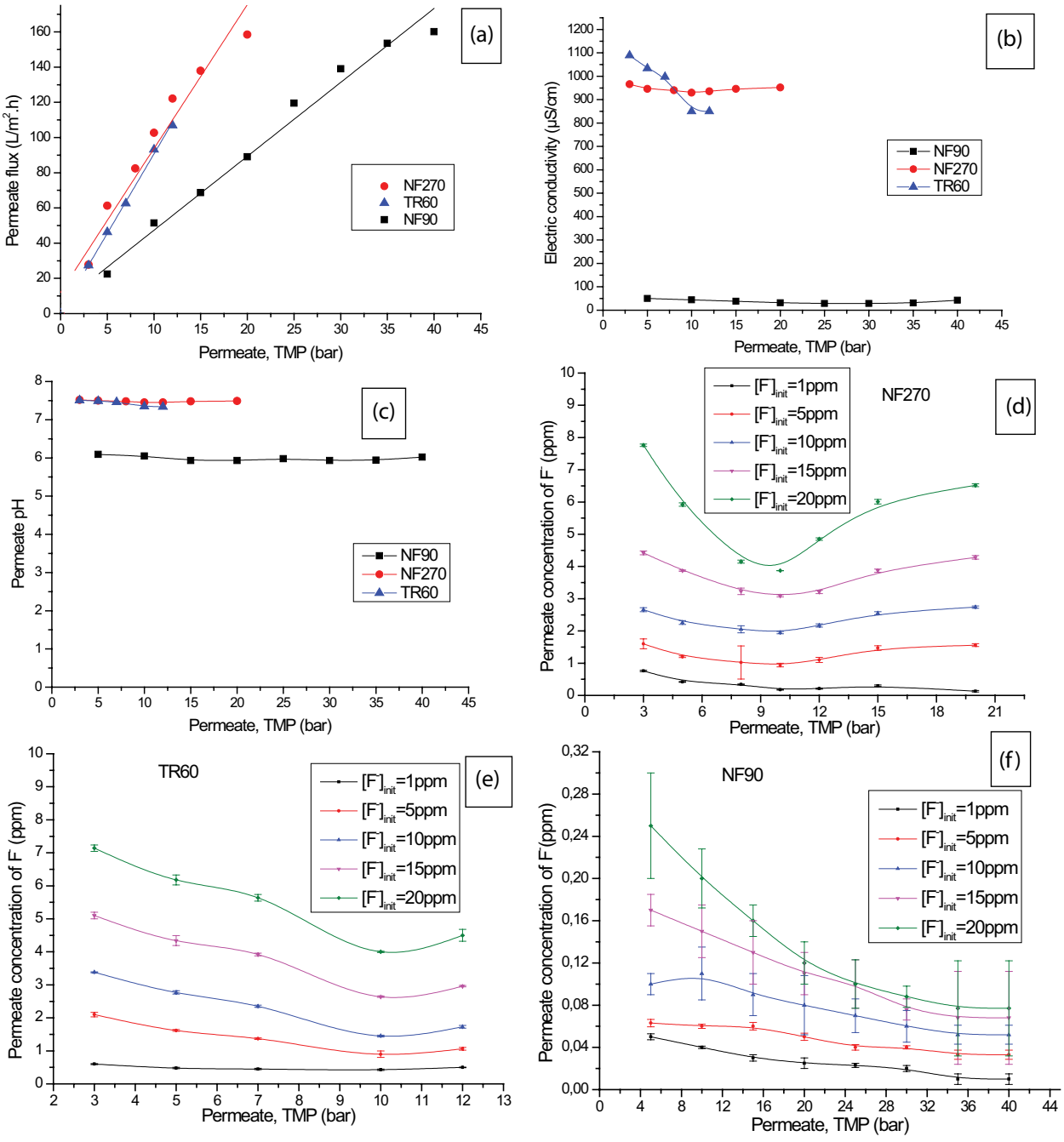

Fig. 2. Variation of (a) the permeate flux, (b) electric conductivity and (c) pH and of permeate fluoride concentration as a function of TMP for different initial feed concentrations.

Pressure improves the driving forces and overcomes the resistance of the membranes [7] resulting in the passage of solute through the membrane. Hence rejection increases with increasing TMP [11]. In this illustration, NF270 exhibits the maximum flux, followed by TR60 and NF90. This order is attributed to the nature of the membranes, NF270 and TR60 have porous structures while NF90 is almost denser [6]. The permeate flow follows the following order: NF270 > TR60 > NF90.

A small variation in pH is observed for the three membranes (Fig. 2d). However, pH values found for NF90 are slightly smaller than that found for TR60 and NF270, this is related to the ratio (HCO_3^-/CO_2) which determines the pH value.

The electric conductivity of the NF90 permeate is very low; remineralization of this water is mandatory if this water is intended for drinking. On the other hand, for the TR60 and NF270, the mineralization obtained is satisfactory.

For the three membranes studied, for the same TMP, the fluoride passage in the permeate increases with the increase in the initial fluoride content in the feed. In addition, for the same initial feed concentration, the fluoride passage in the permeate decreases with increasing TMP, except for NF270, a slight increase is observed for TMP greater than 10 bar. NF90 rejects almost entirely fluoride regardless of the initial fluoride content of the feed water. For NF270 and TR60, the fluoride content obtained is satisfactory for initial feed fluoride concentration less equal or less than 6 ppm. If this concentration is greater than 6 ppm, additional treatment is necessary to bring the fluoride contents back to standards.

4.2. Mathematical models

4.2.1. Mass transfer mechanism

Fig. 3 shows the variation of the concentration of fluoride ion in the permeate as a function of the inverse of the permeate flux according to the equation [Eq. (3)]. The results of Fig. 3 will allow us to understand and determine if the mechanism of fluoride ion transfer in the studied membrane is whether diffusive or convective and to investigate the influence of the initial fluoride feed content on these mechanisms. The intercept allows to know the concentration in the permeate due to convection C_{conv} and the slope allows to determine the flow of solute transported by diffusion J_{diff}. This representation distinguishes and experimentally quantifies the two types of flow. This model allows the separate quantification of the different components of the material transfer of a

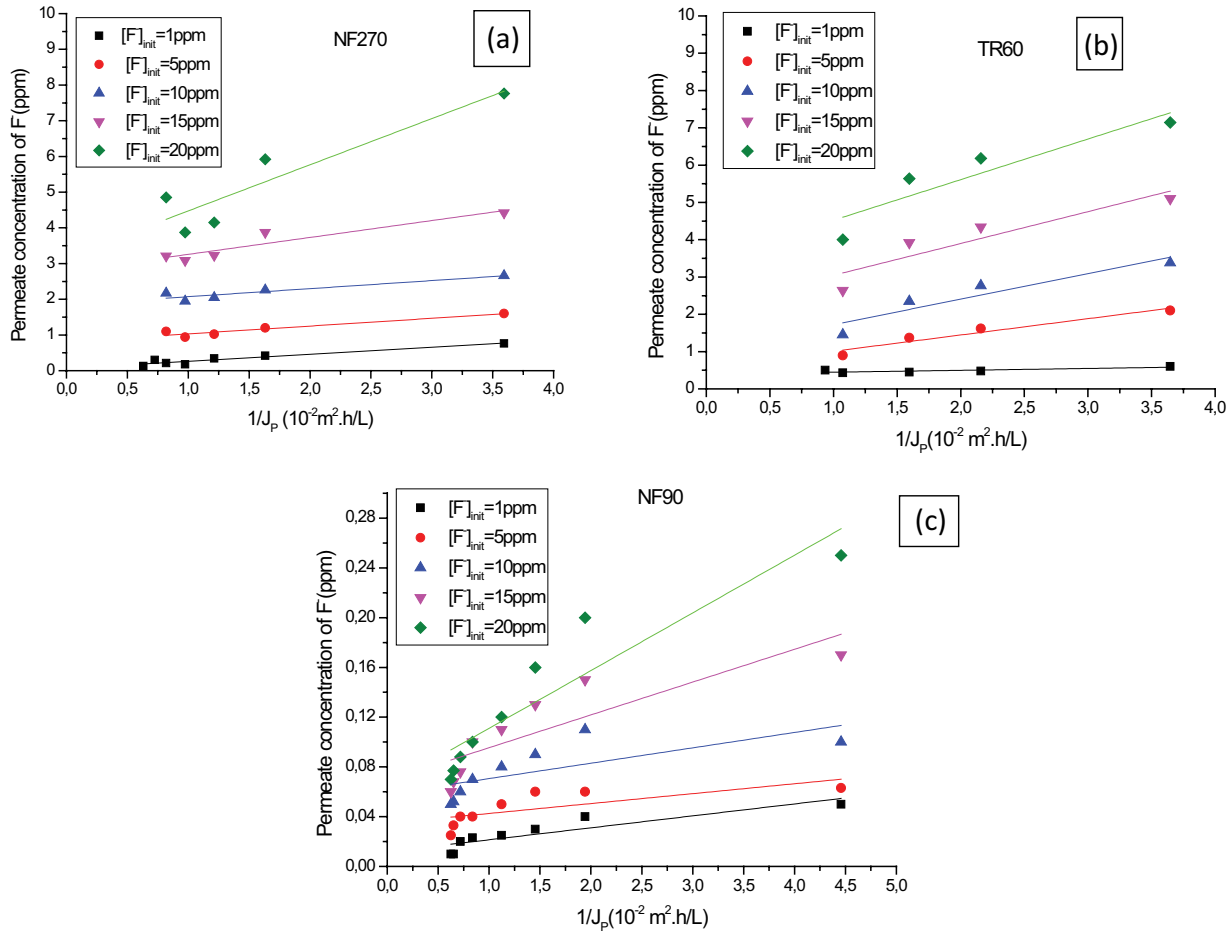

Fig. 3. Permeate concentration of fluoride as a function of the inverse of the flux, for different initial feed concentrations.

solute through NF and *R* membranes [26]. Table 3 gives the values of J_{diff} and C_{conv} for NF270, TR60 and NF90.

As shown in Fig. 3, the variation of the concentration of fluoride ions in the permeate as a function of the inverse of the permeation flow is linear. According to the values in Table 3, C_{conv} and J_{diff} increase with the increase in the initial feed concentration of fluoride. These results show that NF270 and TR60 involve two different mechanisms of transfer, both acting separately, but additively in the global transfer. In comparison TR60 membrane is more diffusive than NF270, this also means that NF270 is more convective than TR60. In addition, the values of C_{conv} are almost close to zero which shows that the diffusion mechanism is predominant. Here is the classification order C_{conv} and J_{diff} for the studied membranes:

$$C_{conv}\text{NF270} > C_{conv}\text{TR60} > C_{conv}\text{NF90} \approx 0$$

$$J_{diff}\text{TR60} > J_{diff}\text{NF270} > J_{diff}\text{NF90}$$

Plotting the evolution of C_{conv} and J_{diff} as a function of the initial concentration of fluoride ions shows how these two parameters are influenced by the initial fluoride content. Fig. 4 shows the variation of the solute flow by convection and the flow by diffusion, as a function of the initial concentration for the three membranes tested.

As shown in Fig. 4, J_{diff} and C_{conv} vary linearly according to the initial feed fluoride concentration. The behavior of NF270 and TR60 are similar, and the slopes of the curves are almost equal. On the other hand, values of J_{diff} and C_{conv} at the origin are different. For NF90, whatever the initial feed fluoride concentration, J_{diff} and C_{conv} remain almost unchanged.

4.2.2. Spiegler–Kedem model fitting

This model is applied for two purposes. The first is to investigate the influence of initial feed fluoride concentration on the permeability of this ion across the three studied membranes, and the second is to quantify the contribution of each transfer mechanism of fluoride. A summary of the calculated transport parameters (reflection coefficient (σ) and the permeability of solute (P_s)) are collected in Table 4.

Fig. 5 shows the variation of the rejection as a function of the permeate flux at various initial concentrations. The result shows a good fit between the experimental and fitting results calculated by the SK model for all the membranes.

Fig. 6 shows the variation of the two determining parameters of the SK model, the permeability of fluoride ions and the reflection coefficient as a function of the initial concentration of fluoride for the three studied membranes. As shown in Fig. 6, the behavior of these two parameters is linear.

The increase in the content of fluoride in raw water causes a slight decline in the permeability of fluoride for the three studied membranes but this decline is more

Table 3
C_{conv} and J_{diff} values obtained at different initial feed fluoride concentration

Initial feed concentration		1 ppm	5 ppm	10 ppm	15 ppm	20 ppm
NF90	C_{conv} (ppm)	0.01181	0.03452	0.05825	0.06905	0.06462
	J_{diff} (m^3 L/h) × 10^{-3}	0.9609	0.79609	1.23609	2.63798	4.64016
	R-square	0.78	0.76	0.71	0.68	0.82
NF270	C_{conv} (ppm)	0.6484	0.81336	1.84701	2.78556	3.18161
	J_{diff} (m^3 L/h) × 10^{-3}	19.67247	21.78385	22.5336	47.28266	129.27804
	R-square	0.90	0.95	0.82	0.85	0.80
TR60	C_{conv} (ppm)	0.39761	0.57203	1.03841	2.1923	3.43423
	J_{diff} (m^3 L/h) × 10^{-3}	5.01555	43.68273	68.39789	85.3242	108.83
	R-square	0.70	0.90	0.81	0.77	0.78

Table 4
Calculated values of σ and P_s by Spiegler–Kedem model

Initial feed fluoride concentration		1 ppm	5 ppm	10 ppm	15 ppm	20 ppm
NF90	P_s (m^3/m^2 s) × 10^{-7}	3.312057	0.60228	0.47514	0.312057	0.72782
	σ	0.98434	0.99186	0.99321	0.99339	0.99564
	R-square	0.99	0.99	0.99	0.99	0.99
NF270	P_s (m^3/m^2 s) × 10^{-6}	–	1.44494	0.6692	0.43388	0.32159
	σ	–	0.75739	0.87876	0.91918	0.939
	R-square	–	0.97	0.99	0.99	0.99
TR60	P_s (m^3/m^2 s) × 10^{-6}	3.72726	4.62735	3.2596	2.8355	2.8136
	σ	0.55651	0.89426	0.89029	0.8355	0.80197
	R-square	0.97	0.99	0.99	0.99	0.99

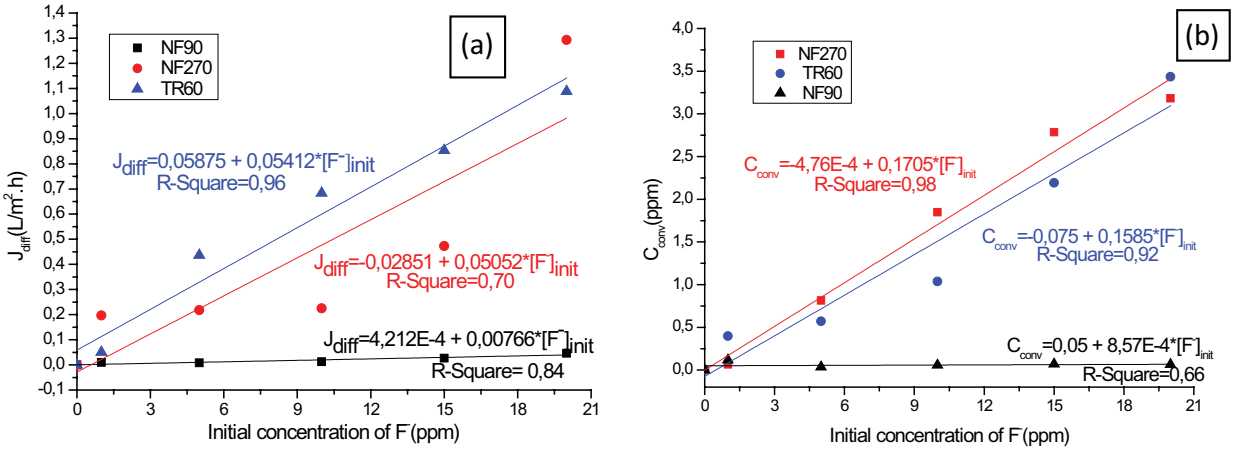

Fig. 4. Variation of diffusion flux J_{diff} (a) and convection concentration (b) of fluoride as a function of initial feed fluoride concentration.

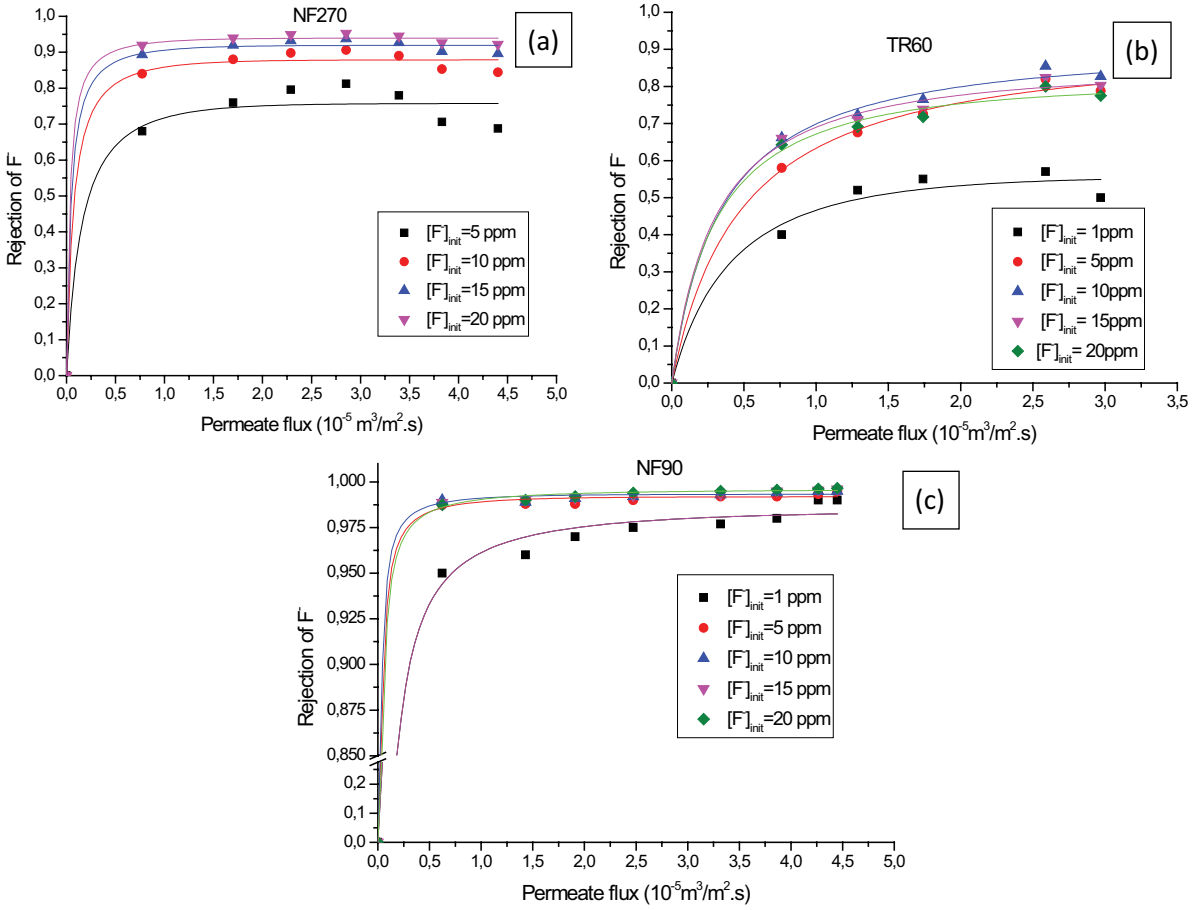

Fig. 5. Experimental and fitting data of fluoride rejection as a function of permeate flux for the three membranes.

pronounced for TR60 and NF270 than for NF90. The average fluoride permeability calculated for the membranes follows the following classification order: TR60 > NF270 > NF90.

The calculated reflection coefficients are almost equal to unity for NF90. For the other two membranes, a slight increase of σ is obtained for NF270 whereas, for TR60, σ decreases with the increase of initial concentration of fluoride.

The reflection coefficient σ obtained for the three membranes follows the following order: NF90 > NF270 > TR60. High reflection coefficients indicate that convective transport in the NF90 membrane is almost completely hampered. For TR60 and NF270 both mechanisms are present with a predominance of diffusion. In reality, the separation mechanism is very complex, in addition to the

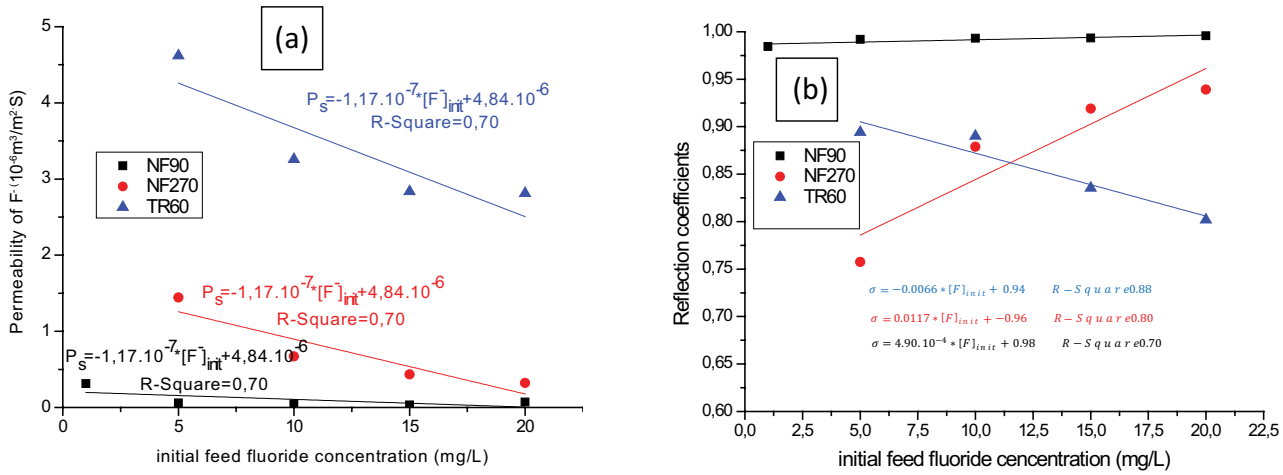

Fig. 6. Permeability fluoride and reflection coefficient as a function of initial feed fluoride concentration for the three membranes.

Table 5
Values of the pore radius for the three membranes studied (r_p)

	r_p (nm)
NF90	0.129
NF270	0.148
TR60	0.167

diffusion, the mechanism includes the dielectric exclusion effect which is caused by the interactions of the ions with the bound electric charges induced by the ions at the interfaces between the media of different dielectric constants, in particular, the membrane matrix and the solvent [27].

4.2.3. Steric Hindrance Pore model

Generally in NF membranes, the high rejection of the fluoride anion is mainly attributed to steric and charging effects [24] at least. The pore size (r_p) remains among the parameters which can illustrate the details of the permeability of the solute through the membrane. The pore radius is determined from the SHP model.

Table 5 gives the mean values of the pore radii for the three membranes studied. Only the value of NF90 is in agreement with the value found in the literature which is 0.12 nm [24]. Luo and Wan [21] found that the r_p of NF270 is 0.43 nm, which is higher than the value obtained by our calculations (r_p = 0.148 nm, whereas the value calculated for TR60 is 0.167. We note that the average of r_p obtained for the membranes tested follows the following order:

$$r_p(\mathrm{TR60}) > r_p(\mathrm{NF270}) > r_p(\mathrm{NF90})$$

For NF270, the difference between the calculated value of the pore radius in this work and in the literature could be explained by the electric interaction between solute and membrane charged surface, a phenomenon that has been neglected in the Kedem–Katchalsky, Speigler–Kedem and SHP models..

For NF90, the obtained result may be justified by the structure of the NF90 which is close to that of RO membranes. The diffusion transport mode of salts through this membrane explains the pore radius value calculated which is in agreement with that found in the literature. In addition, this value shows that the contribution of the effects of the electric interaction in the rejection is minimal.

5. Conclusion

In this work, three NF membranes were studied on real water doped with NaF at different fluoride ion concentrations. The performance comparison of these membranes is carried out to remove fluoride ions in continuous mode. NF90 rejects almost all fluoride ions regardless of the initial fluoride content of the feed water and gave satisfactory results for fluoride removal. For NF270 and TR60, satisfactory fluoride content is obtained for initial fluoride concentration less than or equal to 6 ppm.

The calculated values of C_{conv} and J_{diff} increase with the increase in the initial concentration of fluoride ions. NF270 and TR60 involve two different mechanisms: diffusion and convection. For NF90 the diffusion mechanism is dominant. The classification order of C_{conv} and J_{diff} for the membranes studied is:

$$C_{\mathrm{conv}}\mathrm{NF270} > C_{\mathrm{conv}}\mathrm{TR60} > C_{\mathrm{conv}}\mathrm{NF90} \approx 0.$$

$$J_{\mathrm{diff}}\mathrm{TR60} > J_{\mathrm{diff}}\mathrm{NF270} > J_{\mathrm{diff}}\mathrm{NF90}$$

To study the dependence of the fluoride transfer through these membranes with the initial fluoride concentration detailed description of membrane transport was given by a modification of the Spiegler–Kedem equations. The membrane transport parameters are determined by fitting the Spiegler–Kedem equation for each membrane. Theoretically obtained values show a good correlation with the experimental values. It was shown that the influence of electric interaction in the pores is negligible. The two parameters of the model (σ, P_s) are slightly influenced by the increase in the initial concentration of fluoride ions. The calculated

average solute permeability P_s follows the following order: TR60 > NF270 > NF90.

For the calculated values of reflection coefficient σ, only NF90 has an σ almost close to unity. The classification order for the three membranes is: NF90 > NF270 > TR60

The classification order for pore size (r_p) calculated from the SHP model for the three membranes is:

$$r_p(\mathrm{TR60}) > r_p(\mathrm{NF270}) > r_p(\mathrm{NF90})$$

References

[1] S. Meenakshi, N. Viswanathan, Identification of selective ion-exchange resin for fluoride sorption, J. Colloid Interface Sci., 308 (2007) 438–450.

[2] M. Bodzek, K. Konieczny, Fluorine in the water environment, Desal. Water Treat., 117 (2018) 118–141.

[3] S. Guiza, H. Hajji, M. Bagane, External mass transport process during the adsorption of fluoride from aqueous solution by activated clay, C.R. Chim., 22 (2019) 161–168.

[4] F. Wu, L. Feng, L. Zhang, Rejection prediction of isopropylantipyrine and antipyrine by nanofiltration membranes based on the Spiegler–Kedem–Katchalsky model, Desalination, 362 (2015) 11–17, doi: 10.1016/j.desal.2015.01.046.

[5] S.I. Bouhadjar, H. Kopp, P. Britsch, S.A. Deowan, J. Hoinkis, J. Bundschuh, Solar powered nanofiltration for drinking water production from fluoride-containing groundwater – a pilot study towards developing a sustainable and low-cost treatment plant, J. Environ. Manage., 231 (2019) 1263–1269.

[6] Meenakshi, R.C. Maheshwar, Fluoride in drinking water and its removal, J. Hazard. Mater., 137 (2006) 456–463.

[7] L. Xu, X. Gao, Z. Li, C. Gao, Removal of fluoride by nature diatomite from high-fluorine water: an appropriate pretreatment for nanofiltration process, Desalination, 369 (2015) 97–104.

[8] A. Fatehizadeh, M.M. Amin, M. Sillanpää, N. Hatami, E. Taheri, N. Baghaei, S. Mahajan, Modeling of fluoride rejection from aqueous solution by nanofiltration process: single and binary solution, Desal. Water Treat., 193 (2020) 224–234.

[9] Y. Huang, X. Wang, Y. Xu, S. Feng, J. Liu, H. Wang, Amino-functionalized porous PDVB with high adsorption and regeneration performance for fluoride removal from water, Green Chem. Eng., 2 (2021) 224–232.

[10] M. Tahaikt, S. El-Ghzizel, N. Essafi, M. Hafsi, M. Taky, A. Elmidaoui, Technical-economic comparison of nanofiltration and reverse osmosis in the reduction of fluoride ions from groundwater: experimental, modeling, and cost estimate, Desal. Water Treat., 216 (2021) 83–95.

[11] S.V. Jadhav, K.V. Marathe, V.K. Rathod, A pilot scale concurrent removal of fluoride, arsenic, sulfate and nitrate by using nanofiltration: competing ion interaction and modelling approach, J. Water Process Eng., 13 (2016) 153–167.

[12] K. Wan, L. Huang, J. Yan, B. Ma, X. Huang, Z. Luo, H. Zhang, T. Xiao, Removal of fluoride from industrial wastewater by using different adsorbents: a review, Sci. Total Environ., 773 (2021) 145535, doi: 10.1016/j.scitotenv.2021.145535.

[13] X. Chen, C. Wan, R. Yu, L. Meng, D. Wang, W. Chen, T. Duan, L. Li, A novel carboxylated polyacrylonitrile nanofibrous membrane with high adsorption capacity for fluoride removal from water, J. Hazard. Mater., 411 (2021) 113–125.

[14] S. Chakrabortty, M. Roy, P. Pal., Removal of fluoride from contaminated groundwater by cross flow nanofiltration: transport modeling and economic evaluation, Desalination, 313 (2013) 115–124.

[15] Y.-A. Boussouga, B.S. Richards, A.I. Schäfer, Renewable energy powered membrane technology: system resilience under solar irradiance fluctuations during the treatment of fluoride-rich natural waters by different nanofiltration/reverse osmosis membranes, J. Membr. Sci., 617 (2021) 118452, doi: 10.1016/j.memsci.2020.118452.

[16] M. Tahaikt, A. Ait Haddou, R. El Habbani, Z. Amor, F. Elhannouni, M. Taky, M. Kharif, A. Boughriba, M. Hafsi, A. Elmidaoui, Comparison of the performances of three commercial membranes in fluoride removal by nanofiltration. Continuous operations, Desalination, 225 (2008) 209–219.

[17] J. Shen, A.I. Schäfer, Factors affecting fluoride and natural organic matter (NOM) removal from natural waters in Tanzania by nanofiltration/reverse osmosis, Sci. Total Environ., 527–528 (2015) 520–529.

[18] A. Ben Nasr, C. Charcosset, R. Ben Amar, K. Walha, Defluoridation of water by nanofiltration, J. Fluorine Chem., 150 (2013) 92–97.

[19] J. Hoinkis, S. Valero-Freitag, M.P. Caporgno, C. Pätzold, Removal of nitrate and fluoride by nanofiltration – a comparative study, Desal. Water Treat., 30 (2011) 278–288.

[20] J. Luo, Y. Wan, Effect of highly concentrated salt on retention of organic solutes by nanofiltration polymeric membranes, J. Membr. Sci., 372 (2011) 145–153.

[21] J. Shen, G. Mkongo, G. Abbt-Braun, S.L. Ceppi, B.S. Richards, A.I. Schäfer, Renewable energy powered membrane technology: fluoride removal in a rural community in northern Tanzania, Sep. Purif. Technol., 149 (2015) 349–361.

[22] O. Kedem, A. Katchalsky, Thermodynamic analysis of the permeability of biological membranes to non-electrolytes, Biochim. Biophys. Acta, 27 (1958) 229–246.

[23] K.S. Spiegler, O. Kedem, Thermodynamics of hyperfiltration (reverse osmosis): criteria for efficient membranes, Desalination, 1 (1966) 311–326.

[24] A. Jeihanipour, J. Shen, G. Abbt-Braun, S.A. Huber, G. Mkongo, A.I. Schäfer, Seasonal variation of organic matter characteristics and fluoride concentration in the Maji ya Chai River (Tanzania): impact on treatability by nanofiltration/reverse osmosis, Sci. Total Environ., 637–638 (2018) 1209–1220.

[25] R.R. Nair, E. Protasova, S. Strand, T. Bilstad, Implementation of Spiegler–Kedem and Steric Hindrance Pore Models for analyzing nanofiltration membrane performance for smart water production, Membranes, 8 (2018) 78, doi: 10.3390/membranes8030078.

[26] S.M. Lo, M. Am, K. Courfia, C.K. Diawara, M. Pontié, A.K. Mahmoud, O. Mahmoud, M.L. Fagel, M. Ndongo, M. Rumeau, Caractérisation et Modélisation du Transfert de Matière de Membranes de Nanofiltration (NF) et d'Osmose Inverse (OI) Commerciales: Application au Dessalement Sélectif d'une Eau Faiblement Saumâtre de Mauritanie, J. Soc. Ouest-Afr. Chim., 25 (2008) 19–33.

[27] E. Taheri, S. Hadi, M. Mehdi Amin, A. Ebrahimi, A. Fatehizadeh, T.M. Aminabhavi, Retention of atenolol from single and binary aqueous solutions by thin film composite nanofiltration membrane: transport modeling and pore radius estimation, J. Environ. Manage., 271 (2020) 111005, doi: 10.1016/j.jenvman.2020.111005.